PHYSICAL REVIEW LETTERS **130,** 195101 (2023)

Editors' Suggestion **Featured in Physics**

Characterization of Quasi-Keplerian, Differentially Rotating, Free-Boundary Laboratory Plasmas

V. Valenzuela-Villaseca,[1,*,†] L. G. Suttle,[1] F. Suzuki-Vidal,[1,‡] J. W. D. Halliday,[1] S. Merlini,[1] D. R. Russell,[1]
E. R. Tubman,[1,∥] J. D. Hare,[1,§] J. P. Chittenden,[1] M. E. Koepke,[2] E. G. Blackman,[3] and S. V. Lebedev[1]
[1] *Blackett Laboratory, Imperial College London, London SW7 2BW, United Kingdom*
[2] *Department of Physics, West Virginia University, Morgantown, West Virginia 26506, USA*
[3] *Department of Physics and Astronomy, University of Rochester, Rochester, New York 14627, USA*

(Received 22 December 2021; accepted 29 March 2023; published 12 May 2023)

We present results from pulsed-power driven differentially rotating plasma experiments designed to simulate physics relevant to astrophysical disks and jets. In these experiments, angular momentum is injected by the ram pressure of the ablation flows from a wire array Z pinch. In contrast to previous liquid metal and plasma experiments, rotation is not driven by boundary forces. Axial pressure gradients launch a rotating plasma jet upward, which is confined by a combination of ram, thermal, and magnetic pressure of a surrounding plasma halo. The jet has subsonic rotation, with a maximum rotation velocity 23 ± 3 km/s. The rotational velocity profile is quasi-Keplerian with a positive Rayleigh discriminant $\kappa^2 \propto r^{-2.8\pm0.8}$ rad^2/s^2. The plasma completes 0.5–2 full rotations in the experimental time frame (∼150 ns).

DOI: 10.1103/PhysRevLett.130.195101

Differentially rotating magnetohydrodynamical (MHD) accretion flows orbiting a central object are ubiquitous in the Universe [1,2]. The observational evidence of accretion toward the central object requires angular momentum transport to be far more efficient than can be provided by kinematic viscosity. The enhancement is often modeled as anomalous turbulent viscosity [3]. However, the Rayleigh criterion guarantees the hydrodynamical stability of Keplerian flows since they have a specific angular momentum distribution $\ell(r)$ increasing with radius as $\ell = \Omega r^2 \propto r^{1/2}$ (r is the radial position and Ω the angular frequency) [4]. Luckily, a magnetized flow with the same rotation profile is unstable to the magnetorotational instability (MRI) [5–7], which is triggered when a differentially rotating flow has an angular frequency stratification that monotonically decreases with radius. Indeed, Keplerian flows satisfy $\Omega \propto r^{-3/2}$.

Existing laboratory experiments use the Taylor-Couette geometry to realize steady-state rotating MHD flows and study instabilities, turbulence, and angular momentum transport developing gradually over hundreds of rotation periods. These experiments control the rotation profile from the edges of the flow, either by spinning the vessel containing a liquid (such as water or aqueous glycerol [8], or sodium or gallium alloys under an external magnetic field [9–15]), or by applying electrical currents from the edge of Hall plasmas confined by permanent magnets at the boundary [16–18].

In this Letter, we present results from the Rotating Plasma Experiment (RPX), a novel pulsed-power driven platform to study free-boundary differentially rotating plasmas. The flow is quasi-Keplerian, i.e., $d\Omega/dr < 0$ and $d\ell/dr > 0$, and allows the development of effects with growth times comparable to the rotation period (e.g., the MRI [6]). The measured Rayleigh discriminant [19] is $\kappa^2 \propto r^{-2.8\pm0.8}$ rad^2/s$^2 > 0$. Thus, the flow rotation profile meets the conditions to generate the MRI in a collisional plasma. Additionally, the free-boundary design allows the formation of axial plasma jets launched from the ends of the plasma column, without the flow perturbations characteristic of rigid wall containment [20–23]. The axial jet rotates at a maximum velocity $\gtrsim 20$ km/s, undergoing between 0.5 and 2 full rotations for the duration of the experiment.

The experimental platform inertially drives a rotating plasma by the oblique collision of multiple plasma jets [24], which continuously inject both mass and angular momentum to a rotating plasma column on the axis, as shown in Fig. 1(a). On RPX, the colliding jets are ablation flows accelerated by a cylindrical aluminium wire array (eight 40 μm wires, 16 mm diameter, 10 mm high) [25–27], as shown in Fig. 1(b), driven on the MAGPIE pulsed-power generator (1.4 MA peak electrical current, 240 ns rise time) [28]. Aluminum plasma ablation flows have densities of a few 10^{18} cm^{-3}, and propagate with hypersonic velocities $4 \times 10^4 - 1 \times 10^5$ m/s and characteristic temperature $T \sim 10$ eV (sonic Mach number $M_s > 5$) [29–31]. Angular momentum is introduced by the inward, off-axis trajectory

---

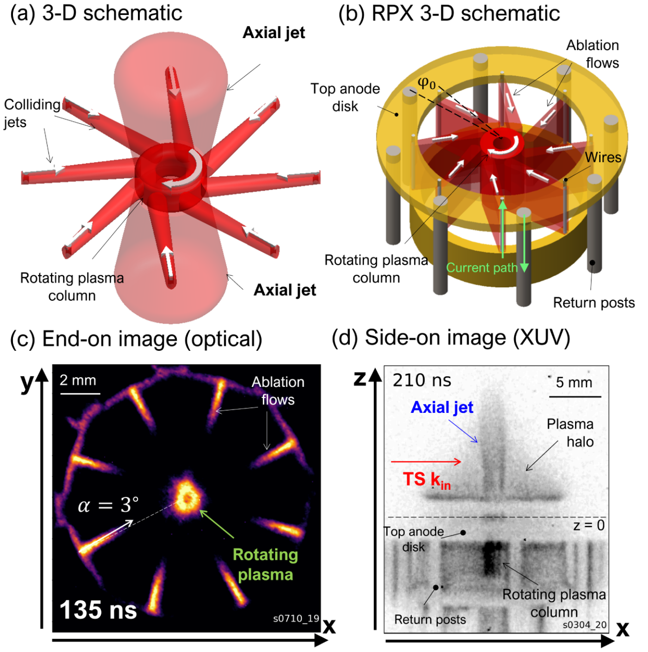

FIG. 1. Schematic diagrams of experimental setup and self-emission images. (a) 3D schematic of inertially driven rotating plasmas. (b) 3D schematic of experimental hardware. Axial jets are not shown. (c) End-on optical self-emission image. (d) Extreme ultraviolet (XUV) image of rotating plasma.

of the ablation flows (described by the propagation angle α), which is set by the ratio of radial-to-azimuthal magnetic field components created by the applied current evaluated at each wire. The azimuthal component $B_\theta \approx 10$ T is mainly generated by the current passing through the wires, whereas the radial component $B_r \approx 2$ T is introduced by return posts slightly offset relative to the wires by an angle $\varphi_0 = 13°$ which carry the electrical current in the opposite direction [Fig. 1(b)]. The experimental total time frame is limited by the initial wire array mass [32], and corresponds to 270 ns for the experiments presented in this Letter.

In each experiment, measurements of the temporal evolution of the plasma density, temperature, and velocity are obtained by using a multidiagnostic suite consisting of self-emission (optical and XUV, 5 ns time resolution) and laser probing [interferometry and optical Thomson Scattering (TS)] [31,33,34].

Figure 1(c) shows one of the end-on optical self-emission images (5 ns resolution, > 600 nm) of the ablation flows and the formation of the rotating plasma. The ablation flows propagate inward, with an offset propagation angle $\alpha = 3° \pm 1°$ [Fig. 1(c)]. As the ablation flows propagate inward, their emission reduces due to radiative cooling [35]. Considering the ablation velocity $V_{ab} = 6 \times 10^4$ m/s [29] and array radius $r = 8 \times 10^{-3}$ m, the specific angular momentum introduced by each wire ablation is $\ell = rV_{ab}\sin(\alpha) = 25 \pm 10$ m^2/s. The 12 optical self-emission images obtained from each experiment indicate that α can slightly vary by $\sim 1°$ between ablation flows in the same experiment due to uneven current distribution through the load.

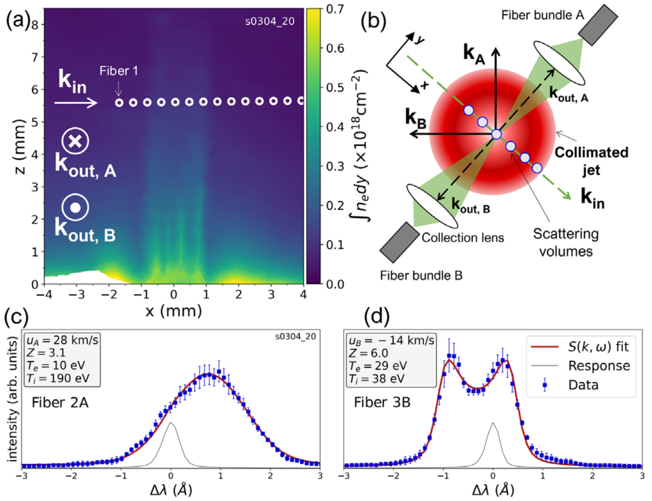

FIG. 2. (a) Line integrated electron density map. TS volumes are overlaid in white circles. Additional arrows indicate the scattering geometry. (b) Schematic TS setup and vector diagram. (c) TS spectrum from outside the jet (plasma halo). Best fit is shown in red. The spectrometer response is shown in gray. Fitting parameters shown in gray box. (d) TS spectrum from inside the jet. The characteristic double peak of the ion-acoustic wave feature is observed.

The formation of the rotating plasma is shown in Fig. 1(c), observed as a bright ring with a reduced intensity on axis. This structure is consistent with a dense plasma shell with a density depletion on axis sustained by a centrifugal barrier. Thus, the plasma accumulates where the centrifugal force is balanced by the inward ram pressure of the ablation flows. This hollow structure is sustained from 130 ns (formation time) to 210 ns.

Above the array, axial plasma outflows are observed by a pair of four-frame, XUV cameras (100 μm pinhole, 1 μm Mylar filter, > 40 eV photon energy, 5 ns time resolution), as shown in Fig. 1(d). A highly collimated jet is launched by axial thermal and magnetic pressure gradients from the formed rotating plasma column. By tracking the jet length across different frames, the estimated axial velocity is $u_z = 100 \pm 20$ km/s. The jet has a divergence angle of $3° \pm 1°$, and there is no visible development of typical MHD instabilities of Z pinch plasmas [36,37], prior to 270 ns. The axial jet is surrounded by a plasma halo, indicated in Fig. 1(d).

Measurements of the outflow's electron density were obtained using a Mach-Zehnder interferometer (532 nm wavelength, 0.5 ns FWHM), with the probing beam passing side on. The raw inteferogram was analyzed using the MAGIC2 code [31,38] to construct a line-integrated electron density $\int n_e dy$ map of the outflows, presented in Fig. 2(a). Our coordinate system is such that the height

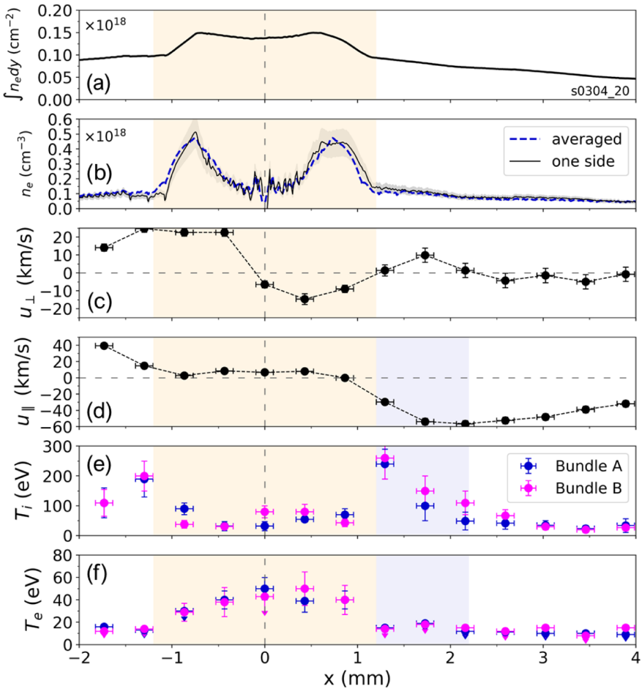

FIG. 3. Plasma parameters. (a) Line-integrated electron density lineout at the same height as the scattering volumes. Uncertainty was estimated to be 20%. (b) Abel inverted electron density. Left- and right-hand-side inversions (black lines) and averaged inversion (dashed blue line). (c) Rotation velocity. (d) Radial velocity. (e) Ion temperature. (d) Electron temperature. Downward pointing arrows indicate the value is an upper constraint.

$z = 0$ coincides with the upper surface of the top anode disk.

A characterization of the density profile, velocity components in the plane of rotation, and ion and electron temperature of the outflows is presented in Fig. 3. A line-integrated electron density lineout at the height of the TS measurements [see Fig. 2(a)] is presented in Fig. 3(a). The lineout was Abel inverted using a onion-peeling method [39] independently on each side of the rotation axis, and then the two sides are averaged, to obtain an electron number density. The density profile of the plasma in this region consists of an outer plasma halo at $\sim 0.2 \times 10^{18}$ cm^{-3} surrounding a hollow axial jet of maximum density $\sim 0.5 \times 10^{18}$ cm^{-3} on the shell and axial density comparable to the halo.

Local measurements of velocity in the plane of rotation and temperature are obtained using the TS diagnostic. Scattered spectra are collected from 40 200 μm diameter scattering volumes located across the collimated jet and the surrounding plasma halo, as shown in Fig. 2(a). The scattered light is collected by two linear arrays of 100 μm diameter optic fibers (labeled A and B), located at ±90° relative to the probing wave vector k_{in}, as shown in Fig. 2(b). Fits of the TS spectra [Figs. 2(c) and 2(d)] yield measurements of the velocity components along the scattering vectors $\mathbf{k_A} \equiv \mathbf{k_{out,A}} - \mathbf{k_{in}}$ and $\mathbf{k_B} \equiv \mathbf{k_{out,B}} - \mathbf{k}_{\text{in}}$, and the temperature T_i and the product of the average charge state and electron temperature ZT_e. This product is decoupled using the non local thermodynamic equilibrium code SpK [40,41]. The fit uses the electron density obtained from interferometry shown in Fig. 3(b). From the velocity components $u_{A,B} \equiv \mathbf{u} \cdot \mathbf{k_{A,B}}$, the new components, along and perpendicular to $\mathbf{k_{in}}$ are calculated as

$$u_\parallel = -\frac{1}{\sqrt{2}}(u_A + u_B), \qquad u_\perp = \frac{1}{\sqrt{2}}(u_A - u_B). \tag{1}$$

The laser beam passes approximately through the rotation axis with Fiber 5 viewing the position $x = 0$ with an estimated accuracy of 200 μm; however we cannot exclude an offset of the jet in the perpendicular, y direction [(out of plane in Fig. 2(a)]. If there is no offset of the probe beam along y, the absolute values of the components $(u_\parallel, u_\perp)$ correspond exactly to the radial and rotation velocity components (u_r, u_θ). We show below that the interpretation of the data is not sensitive to the offset of the beam relative to the axial jet along the y axis.

The rotation velocity distribution is shown in Fig. 3(c). Inside the jet, rotation is manifested as the change in sign in the velocity about the axis [orange region in Fig. 3(c)] exhibiting a maximum velocity of 23 ± 3 km/s. The flow velocity distribution is not symmetric about the jet axis. Nonaxisymmetric modulations could be imprinted from the discrete nature of the driver, i.e., the eight ablation flows. Since the ablation geometry is steady, we do not expect the nonaxisymmetric features to evolve significantly throughout the experimental time frame. Figure 3(d) shows the radial component of velocity. The plasma from the halo propagates inward at a maximum velocity of 45 ± 5 km/s, before decelerating in the vicinity of the jet. We call this the deceleration region [blue region in Fig. 3(d)]. This component reaches a minimum inside of the jet, pointing along $\mathbf{k_{in}}$, which indicates that the probe beam is misaligned with the rotation axis.

Ion and electron temperature distributions obtained by fitting the spectra from each fiber bundle independently are shown in Fig. 3(e). At large radii ($x > 3$ mm) $T_i \approx T_e = 10 \pm 3$ eV and gradually increase as the plasma approaches the deceleration region. However, at the deceleration region, the ion temperature of the inflowing plasma increases by a factor of 5 over a length ~1 mm, reaching $T_i = 250 \pm 50$ eV, whereas the electrons increase to $T_e \lesssim 20$ eV. It is inferred that the inflow undergoes a transonic deceleration: from a sonic Mach number $M_s \sim 3$ at $x = 2.5$ mm, to $M_s \lesssim 1$ in the deceleration region. The electron-ion equilibration time in the deceleration region $\bar{\nu}_{e\backslash i}^{-1} = 20 \pm 5$ ns [42], equal to the transit time in this region.

Inside the jet, T_i ranges between 50 ± 15 eV and 100 ± 20 eV, whereas T_e ranges between $\sim 30 \pm 5$ eV

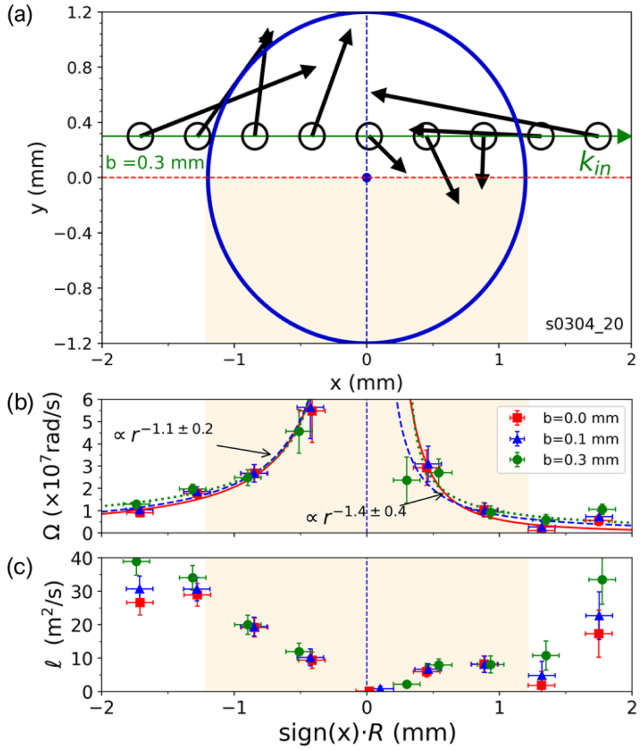

FIG. 4. Rotation velocity distribution depending on TS beam impact parameter b. (a) Diagram of the velocity map (black arrows) of each TS volume (black circles). Example impact parameter $b = 0.3$ mm is shown. (b) Angular frequency distribution. (c) Angular momentum distribution.

and 50 ± 10 eV, exhibiting a gradual increase toward the axis. This increase T_e is consistent with efficient electron-ion thermal equilibration ($\bar{\nu}_{e\backslash i}^{-1} = 18 \pm 5$ ns). However, radiative cooling prevents full equilibration as the radiative cooling time is $\tau_{\mathrm{cool}} \sim 10$ ns [43,44] ($\approx \bar{\nu}_{e\backslash i}^{-1}$), keeping the electrons thermally uncoupled to the ions. The inferred rotational Mach number $M_s \sim 0.8$.

Further characterization of the velocity distribution is presented. Figure 4(a) shows an end-on 2D velocity map constructed from the TS measurements, where the positions of the scattering volumes are translated according to an impact parameter b, defined as the orthogonal distance from the probing beam to the rotation axis (i.e., along y). The scattering volumes are located at positions x_i along the x axis; thus the angular frequency at radius $R_i = \sqrt{x_i^2 + b^2}$ is given by

$$\Omega(R_i) = \frac{x_i u_\perp - b u_\parallel}{R_i^2}. \qquad (2)$$

Figure 4(b) shows the calculated angular frequency distributions for three values of the impact parameter: $b = 0$ mm (i.e., beam passing through the rotation axis), $b = 0.1$ mm, and $b = 0.3$ mm. The result shows the distribution does not significantly change with the impact parameter. The angular frequency distribution for each value of b is fitted independently either side of the axis using a power law $\propto r^\gamma$. For the case $b = 0$, the point closest to the axis was not considered. The variation of values of b was used to find a range of values of γ indicated in the figure. The Rayleigh discriminant can be calculated as $\kappa^2 \equiv r^{-3} d(r^4\Omega^2)/dr \propto (4+2\gamma) r^{2\gamma} = r^{-2.8\pm0.8} > 0$. The physical meaning of this value of κ^2 is twofold. Firstly, its positive value implies that the flow is hydrodynamically stable against axisymmetric perturbations. This is because a linearly perturbed trajectory would oscillate around an unperturbed one (having the same initial conditions) with frequency κ, termed epicyclic frequency [45]. Nonaxisymmetric modes are unstable when $\ell(r) =$ constant, which is not satisfied by our plasma [see Fig. 4(c)] [45,46]. Secondly, a magnetized, rotating flow can be MRI unstable when $d\Omega/dr < 0$. It is explicit from the definition of κ^2 that both hydrostability and magnetorotational instability are satisfied simultaneously when $-2 < \gamma < 0$. This case is called quasi-Keplerian rotation. In that sense, κ^2 fully characterizes the differential rotation profile.

The viscous and resistive diffusion length scales, defined such that the magnetic and fluid Reynolds numbers are of order unity [42,47], are $\ell_\eta \sim 70$ μm and $\ell_\nu \sim 0.5$ μm respectively. They are much smaller than both the plasma length and diameter. In fact, by considering the diameter as a relevant length, the fluid and magnetic Reynolds take minimum characteristic values of $\mathrm{Re} \sim 10^4$ and $\mathrm{Rm} \sim 30$ meaning that dissipation is negligible in the experimental time frame. Thus, in the presence of an external vertical field (absent in these experiments), the MRI's fastest growing mode would develop on timescales $|\omega_{\max}|^{-1} = |\kappa^2/4\Omega - \Omega|^{-1} = 150 \pm 100$ ns, comparable to the orbital period [45]. Therefore, these experiments demonstrate that this free-boundary laboratory platform is able to produce rotating flows with the correct profile and fluid conditions to generate the linear MRI in a pulsed-power plasma. The minimum external magnetic field required can be estimated by imposing that the fastest growing mode can overcome magnetic diffusion $k_z \sim \Omega/V_A > \Omega/\eta$ (where V_A is the vertical Alfvén velocity) [6], which yields a minimum external field in the range $B_z \sim 0.5$–5 T, depending on the plasma density. Moreover, the presence of axial jets might help the instability growth if the axial expansion increases the effective scale height more than it decreases the wave number of perturbations, thereby allowing lower wave numbers to become unstable during the duration of the experiment.

In summary, we have presented an experimental characterization of free-boundary rotating laboratory plasmas which launch axial jets with a hollow density structure. The measured rotation velocity profile corresponds to quasi-Keplerian rotation with Rayleigh discriminant

$\kappa^2 \propto r^{-2.8\pm0.8} > 0$, indicating that the flow is hydrodynamically stable but potentially MHD unstable. This is limited to the mass per unit length of each wire, but it can be increased by using wires of greater diameter.

Although current experiments are yet too short lived to reach the MRI nonlinear regime and associated turbulent angular momentum transport, they are a key initial step in establishing a laboratory astrophysics platform for basic investigations of rotating plasma flows. Observation of the linear amplification of an externally applied, initial magnetic field by differential rotation in this platform, let alone the fully developed MRI, would represent a novel proof-of-principle measurement. These results are a first step toward new efforts to generate and study the MRI, dynamo effects, and collimation of jets in a single plasma experiment, where effects such as radiative cooling are important. By changing the wire material, the effect of radiative cooling can be reduced, effectively suppressing magnetic diffusion, and increasing both the plasma temperature, magnetic Reynolds, and magnetic Prandtl numbers. The initial conditions can be designed to produce a larger diameter plasma, which would make it easier to diagnose [48]. Future experiments will study the magnetic field evolution to investigate the existence of shear-flow magnetic dynamo on RPX. Experiments on long-drive pulsed-power generators with microsecond rise times (e.g., Ref. [49]) could sustain five to ten rotations, allowing the experiment to enter the nonlinear, fully turbulent regime, and would allow the assessment of the effect of azimuthal magnetic fields which drive the slowly growing azimuthal MRI [50].

This work was supported in part by NNSA under DOE Cooperative Agreements No. DE-SC0020434 and No. DE-NA0003764. Vicente Valenzuela-Villaseca was funded by the Imperial College President's PhD Scholarships and the Royal Astronomical Society. We are grateful to the Mechanical Workshop at the Imperial College Department of Physics, and in particular to David Williams, for hardware fabrication. We thank Thomas Varnish for writing some of the codes used in the analysis.

---

[*] vv5425@princeton.edu

[†] Current address: Department of Astrophysical Sciences, Princeton University, Princeton, New Jersey 08544, USA.

[‡] Current address: First Light Fusion Ltd., Yarnton, Kidlington OX5 1QU, United Kingdom.

[‖] Current address: Lawrence Livermore National Laboratory, Livermore, California 94550, USA.

[§] Current address: Plasma Science and Fusion Center, Massachusetts Institute of Technology, Cambridge, Massachusetts 02139, USA.

[1] J. E. Pringle, Accretion discs in astrophysics, Annu. Rev. Astron. Astrophys. **19**, 137 (1981).

[2] J. Frank, A. King, and D. Raine, *Accretion Power in Astrophysics*, 3rd ed. (Cambridge University Press, New York, 2002).

[3] N. I. Shakura and R. A. Sunyaev, Black holes in binary systems. Observational appearance, Astron. Astrophys. **24**, 337 (1973), https://ui.adsabs.harvard.edu/abs/1973A%26A....24..337S/abstract.

[4] S. Chandrasekhar, *Hydrodynamic and Hydromagnetic Stability*, 1st ed. (Oxford University Press, New York, 1961).

[5] E. P. Velikhov, Stability of an ideally conducting liquid flowing between cylinders rotating in a magnetic field, Sov. Phys. JETP **36**, 995 (1959), http://www.jetp.ras.ru/cgi-bin/dn/e_009_05_0995.pdf.

[6] S. A. Balbus and J. F. Hawley, A powerful local shear instability in weakly magnetized disks, Astrophys. J. **376**, 214 (1991).

[7] J. Goodman and G. Xu, Parasitic instabilities in magnetized, differentially rotating disks, Astrophys. J. **432**, 213 (1994).

[8] H. Ji, M. Burin, E. Schartman, and J. Goodman, Hydrodynamic turbulence cannot transport angular momentum effectively in astrophysical disks, Nature (London) **444**, 343 (2006).

[9] H. Ji, J. Goodman, and A. Kageyama, Magnetorotational instability in a rotating liquid metal annulus, Mon. Not. R. Astron. Soc. **325**, L1 (2001).

[10] J. Goodman and H. Ji, Magnetorotational instability of dissipative Couette flow, J. Fluid Mech. **462**, 365 (2002).

[11] R. Hollerbach and G. Rüdiger, New Type of Magnetorotational Instability in Cylindrical Taylor-Couette Flow, Phys. Rev. Lett. **95**, 124501 (2005).

[12] F. Stefani, T. Gundrum, G. Gerbeth, G. Rüdiger, M. Schultz, J. Szklarski, and R. Hollerbach, Experimental Evidence for Magnetorotational Instability in a Taylor-Couette Flow Under the Influence of a Helical Magnetic Field, Phys. Rev. Lett. **97**, 184502 (2006).

[13] W. Liu, J. Goodman, I. Herron, and J. Hantao, Helical magnetorotational instability in magnetized Taylor-Couette flow, Phys. Rev. E **74**, 056302 (2006).

[14] Y. Wang, E. P. Gilson, F. Ebrahimi, J. Goodman, K. J. Caspary, H. W. Winarto, and H. Ji, Identification of a non-axisymmetric mode in laboratory experiments searching for standard magnetorotational instability, Nat. Commun. **13**, 1 (2022).

[15] Y. Wang, E. P. Gilson, F. Ebrahimi, J. Goodman, and H. Ji, Observation of Axisymmetric Standard Magnetorotational Instability in the Laboratory, Phys. Rev. Lett. **129**, 115001 (2022).

[16] C. Collins, N. Katz, J. Wallace, J. Jara-Almonte, I. Reese, E. Zweibel, and C. B. Forest, Stirring Unmagnetized Plasma, Phys. Rev. Lett. **108**, 115001 (2012).

[17] K. Flanagan, J. Milhone, J. Egedal, D. Endrizzi, J. Olson, E. E. Peterson, R. Sassella, and C. B. Forest, Weakly Magnetized, Hall Dominated Plasma Couette Flow, Phys. Rev. Lett. **125**, 135001 (2020).

[18] J. Milhone, K. Flanagan, J. Egedal, D. Endrizzi, J. Olson, E. E. Peterson, J. C. Wright, and C. B. Forest, Ion Heating and Flow Driven by an Instability Found in Plasma Couette Flow, Phys. Rev. Lett. **126**, 185002 (2021).

[19] S. A. Balbus, On the behaviour of the magnetorotational instability when the Rayleigh criterion is violated, Mon. Not. R. Astron. Soc. **423**, L50 (2012).

[20] C. Gissinger, H. Ji, and J. Goodman, Instabilities in magnetized spherical Couette flow, Phys. Rev. E **84**, 026308 (2011).

[21] E. M. Edlund and H. Ji, Reynolds number scaling of the influence of boundary layers on the global behavior of laboratory quasi-Keplerian flows, Phys. Rev. E **92**, 043005 (2015).

[22] S. A. Balbus, When is high Reynolds number shear flow not turbulent?, J. Fluid Mech. **824**, 1 (2017).

[23] K. J. Caspary, D. Choi, F. Ebrahimi, E. P. Gilson, J. Goodman, and H. Ji, Effects of axial boundary conductivity on a free Stewartson-Shercliff layer, Phys. Rev. E **97**, 063110 (2018).

[24] D. D. Ryutov, Using intense lasers to simulate aspects of accretion discs and outflows in astrophysics, Astrophys. Space Sci. **336**, 21 (2011).

[25] M. Bocchi, J. P. Chittenden, S. V. Lebedev, G. N. Hall, M. Bennett, A. Frank, and E. G. Blackman, Numerical simulations of Z-pinch experiments to create supersonic differentially-rotating plasma flows, Astrophys. J. **767**, 84 (2013).

[26] M. Bocchi, J. P. Chittenden, S. V. Lebedev, G. N. Hall, M. Bennett, A. Frank, and E. G. Blackman, Numerical simulations of Z-pinch experiments to create supersonic differentially-rotating plasma flows, High Energy Density Phys. **9**, 108 (2013).

[27] M. J. Bennett *et al.*, Formation of radiatively cooled, supersonically rotating, plasma flows in Z-pinch experiments: Towards the development of an experimental platform to study accretion disk physics in the laboratory, High Energy Density Phys. **17**, 63 (2015).

[28] I. H. Mitchell, J. M. Bayley, J. P. Chittenden, J. F. Worley, a. E. Dangor, M. G. Haines, and P. Choi, A high impedance mega-ampere generator for fiber z-pinch experiments, Rev. Sci. Instrum. **67**, 1533 (1996).

[29] A. J. Harvey-Thompson *et al.*, Optical Thomson Scattering Measurements of Plasma Parameters in the Ablation Stage of Wire Array Z Pinches, Phys. Rev. Lett. **108**, 145002 (2012).

[30] A. J. Harvey-Thompson *et al.*, Optical Thomson scattering measurements of cylindrical wire array parameters, Phys. Plasmas **19**, 056303 (2012).

[31] G. F. Swadling, S. V. Lebedev, N. Niasse, J. P. Chittenden, G. N. Hall, F. Suzuki-Vidal, G. Burdiak, A. J. Harvey-Thompson, S. N. Bland, P. De Grouchy, E. Khoory, L. Pickworth, J. Skidmore, and L. Suttle, Oblique shock structures formed during the ablation phase of aluminium wire array z-pinches, Phys. Plasmas **20**, 022705 (2013).

[32] S. V. Lebedev, F. N. Beg, S. N. Bland, J. P. Chittenden, A. E. Dangor, M. G. Haines, S. A. Pikuz, and T. A. Shelkovenko, Plasma formation and the implosion phase of wire array z-pinch experiments, Laser Part. Beams **19**, 355 (2001).

[33] G. F. Swadling *et al.*, Diagnosing collisions of magnetized, high energy density plasma flows using a combination of collective Thomson scattering, Faraday rotation, and interferometry (invited), Rev. Sci. Instrum. **85**, 11E502 (2014).

[34] L. G. Suttle, J. D. Hare, J. W. Halliday, S. Merlini, D. R. Russell, E. R. Tubman, V. Valenzuela-Villaseca, W. Rozmus, C. Bruulsema, and S. V. Lebedev, Collective optical Thomson scattering in pulsed-power driven high energy density physics experiments (invited), Rev. Sci. Instrum. **92**, 033542 (2021).

[35] S. V. Lebedev, A. Ciardi, D. J. Ampleford, S. N. Bland, S. C. Bott, J. P. Chittenden, G. N. Hall, J. Rapley, C. Jennings, M. Sherlock, A. Frank, and E. G. Blackman, Production of radiatively cooled hypersonic plasma jets and links to astrophysical jets, Plasma Phys. Controlled Fusion **47**, B465 (2005).

[36] S. C. Bott, S. V. Lebedev, D. J. Ampleford, S. N. Bland, J. P. Chittenden, A. Ciardi, M. G. Haines, C. Jennings, M. Sherlock, G. Hall, J. Rapley, F. N. Beg, and J. Palmer, Dynamics of cylindrically converging precursor plasma flow in wire-array Z -pinch experiments, Phys. Rev. E **74**, 046403 (2006).

[37] F. Veloso, G. Muñoz-Cordovez, L. Donoso-Tapia, V. Valenzuela-Villaseca, F. Suzuki-Vidal, G. Swadling, J. Chittenden, M. Favre, and E. Wyndham, Ablation dynamics in wire array Z-pinches under modifications on global magnetic field topology, Phys. Plasmas **22**, 072509 (2015).

[38] J. D. Hare, J. MacDonald, S. N. Bland, J. Dranczewski, J. W. D. Halliday, S. V. Lebedev, L. G. Suttle, E. R. Tubman, and W. Rozmus, Two-colour interferometry and Thomson scattering measurements of a plasma gun, Plasma Phys. Controlled Fusion **61**, 085012 (2019).

[39] C. J. Dasch, One-dimensional tomography: A comparison of Abel, onion-peeling, and filtered backprojection methods, Appl. Opt. **31**, 1146 (1992).

[40] N.-P. L. Niasse, Development of a pseudo Non-LTE model for Z-pinch simulations, Ph.D. thesis, Imperial College London, 2011.

[41] J. D. Hare, High energy density magnetic reconnection experiments in colliding carbon plasma flows, Ph.D. thesis, Imperial College London, 2017.

[42] J. Huba, *NRL Plasma Formulary*, (Naval Research Laboratory, Washington, DC 2016).

[43] F. Suzuki-Vidal *et al.*, Bow shock fragmentation driven by a thermal instability in laboratory astrophysics experiments, Astrophys. J. **815**, 96 (2015).

[44] D. R. Russell, Bow shock interaction experiments in a magnetised collisional plasma, Ph.D. thesis, Imperial College London, 2021.

[45] S. A. Balbus and J. F. Hawley, Instability, turbulence, and enhanced transport in accretion disks, Rev. Mod. Phys. **70**, 53 (1998).

[46] J. C. B. Papaloizou and J. E. Pringle, The dynamical stability of differentially rotating discs with constant specific angular momentum, Mon. Not. R. Astron. Soc. **208**, 721 (1984).

[47] D. Ryutov, R. Drake, J. Kane, E. Liang, B. A. Remington, and W. M. Wood-Vasey, Similarity criteria for the laboratory simulation of supernova hydrodynamics, Astrophys. J. **518**, 821 (1999).

[48] V. Valenzuela-Villaseca, Experimental study of magneto-inertially driven, differentially rotating plasma flows, Ph.D. thesis, Imperial College London, 2022.

[49] J. T. Banasek, T. G. Oliver, S. W. Cordaro, and S. C. Bott-Suzuki, Free space Thomson scattering to study high energy density shocks, Rev. Sci. Instrum. **92**, 093503 (2021).

[50] G. Rüdiger, M. Gellert, M. Schultz, R. Hollerbach, and F. Stefani, Astrophysical and experimental implications from the magnetorotational instability of toroidal fields, Mon. Not. R. Astron. Soc. **438**, 271 (2014).